Fuel 361 (2024) 130646

Contents lists available at ScienceDirect

Fuel

journal homepage: www.elsevier.com/locate/fuel

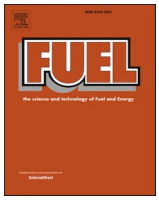

Full Length Article

Azobenzene-equipped Covalent triazine polymers for Visible-Light-Driven photocatalytic reduction of CO_2 to CH_4

Qi Huang [a], Zhen Zhan [b], Yuanting Qiao [a], Xueting Pan [a], Shaojun Xu [c,d,e], Bien Tan [b,*], Chunfei Wu [a,*]

[a] School of Chemistry and Chemical Engineering, Queen's University Belfast, Belfast BT7 1NN, UK
[b] Key Laboratory of Material Chemistry for Energy Conversion and Storage, Ministry of Education, School of Chemistry and Chemical Engineering, Huazhong University of Science and Technology, Luoyu Road No. 1037, Wuhan 430074, China
[c] Department of Chemical Engineering, University of Manchester, Manchester M13 9PL, UK
[d] UK Catalysis Hub, Research Complex at Harwell, Rutherford Appleton Laboratory, Harwell OX11 0FA, UK
[e] School of Chemistry, Cardiff University, Cardiff CF10 3AT, UK

ARTICLE INFO

Keywords:
Azobenzene contained
Covalent triazine polymers (CTPs)
photocatalytic CO_2 conversion

ABSTRACT

Covalent triazine polymers, as large π conjugated, highly porous, nitrogen riched organic semiconductors, can play a key role in tackling the fuel energy crisis and global warming issues. However, their development in photocatalytic CO_2 reduction is still rare. More effective strategies to enhance CO_2 reduction activity need to be explored. Herein, different amounts of azobenzene pendants functionalized CTPs: Azo-CTP_0, Azo-CTP_1, Azo-$mCTP_1$ and Azo-CTP_2, were fabricated for photocatalytic CO_2 reduction with Pd loaded. Among them, Azo-$mCTP_1$ displayed the highest CO_2 uptake capacity up to 48.2 $cm^3\ g^{-1}$ (2.15 mmol g^{-1}) at 273 K, and the highest CH_4 evolution rate in the water system, with selectivity highly up to 97 %. Apart from that, the azobenzene functionalization of Azo-CTP_0 could significantly boost the CO_2 reduction efficiency by 4 times. Therefore, this study provides a potentially general approach for accurately modifying organic semiconductors to enhance photocatalytic performance.

1. Introduction

Great efforts have been carried out to tackle current environmental issues and energy shortage problems caused by uncontrolled energy consumption and excessive CO_2 emissions, such as using renewable energy resources for valuable chemical fuels.[1–3] Visible light triggered CO_2 reduction into fuels like methane has attracted tremendous interest because of the double benefits of providing useful carbon energy and the maintenance of world carbon balance. [4–6] To date, many semiconductors have been fabricated for photocatalytic CO_2 reduction and are mostly concentrated on inorganic photocatalysts.[7] However, these inorganic semiconductors are restricted by the low adsorption capacity of CO_2 and the difficulty of structural modulation, which significantly limits the improvement of photocatalytic CO_2 reduction efficiency.[8].

Covalent triazine polymers (CTPs) [9], as a kind of wild reported organic photocatalysts, comprise various superior properties, such as a large π conjugated system, high surface area, rich nitrogen content as well as high thermal stability for repeated applications.[10–12] Such properties endow them with a strong affinity toward CO_2 molecules [13–15] and a broad visible light absorption range.[16] Moreover, the structural variety and tunability of CTPs enable easy modification of electronic properties and band gap structures,[17] which are of vital importance to photocatalytic performance.[18–20] However, the research on CTPs applied in photocatalytic reduction of CO_2 to CH_4 is still challenging due to the requirement of a strong driving force to active CO_2 molecules with 8 electrons. For instance, Wu et al. reported a platinum single-atoms anchored CTP for photocatalytic CO_2 reduction. [21] However, the CO_2 uptake capacity of Pt-SA/CTF-1 was only 8.2 cm^3/g while the CH_4 evolution rate in the water system was also only 4.5 μmol/g/h under visible light irradiation. Thus, a new type of CTP system that permits the efficient optimization of photocatalytic CO_2 reduction to CH_4 is urgently required.[21–23].

In the meantime, azo-based porous polymers are emerging with great attention.[24–26] Owning to the CO_2 affinity property of azo groups combined with high surface area, incorporating azo benzene groups into

* Corresponding authors.
E-mail addresses: bien.tan@mail.hust.edu.cn (B. Tan), c.wu@qub.ac.uk (C. Wu).

https://doi.org/10.1016/j.fuel.2023.130646
Received 17 September 2023; Received in revised form 28 November 2023; Accepted 12 December 2023
Available online 28 December 2023

polymer materials can achieve high CO_2 adsorption capacity.[27] Furthermore, when combined with catalytic species, such bifunctional materials can further exhibit strong potential for the application of CO_2 capture and conversion.[28–30] For instance, Zhang et al.[31] fabricated an azo-linked framework, and the CO_2 adsorption capacity was up to 18.2 wt%. Furthermore, after being loaded with $ZnBr_2$, high catalytic activity for CO_2 conversion to carbonates has been achieved. Therefore, different sites or amounts of azobenzene functionalization could be an effective way to both tune the CO_2 uptake capacity and tailor the band gap structure of CTP semiconductors for optimized photocatalytic CO_2 conversion activity.

Herein, a series of different content of azobenzene functionalized Azo-CTPs were fabricated. In detail, Azo-CTP_0, Azo-CTP_1 and Azo-CTP_2 were synthesized from the aldehyde monomers containing zero (M_0), one (M_1) and two (M_2) azobenzene pendants, respectively. In addition, Azo-mCTP_1 was also designed from the further shape adjusting of M_1 to mM_1. Thus, the azobenzene content and sites were tuned to modify the surface area and band gap structure of the materials. Results suggested that the azobenezene incorporation successfully improve the CO_2 uptake capacity up to 48.2 $cm^3\ g^{-1}$ (2.15 mmol g^{-1}) of Azo-mCTP_1 at 273 K. Moreover, after being loaded with palladium as cocatalyst, such azo-based CTPs were then applied to the visible light induced photocatalytic CO_2 reduction in the water solution system. Through azobenzene functionalization, Azo-mCTP_1 suggested the highest CO_2 uptake capacity and the highest CO_2 reduction efficiency that can reduce CO_2 to CH_4 with selectivity up to 97 %. The azobenzene installation successfully modified the CO_2 uptake capacity and band gap structure of Azo-CTPs and contributed to the highest CO_2 capture and conversion efficiency of Azo-mCTP_1.

2. Experimental section

2.1. Materials and characterization

2, 5-dibromoaniline, Nitrosobenzene, 3,5-Dibromoaniline, 2, 5-Dibromobenzene-1,4-diamine, bis(triphenylphosphine) palladium(II) dichloride and 4-formylphenylboronic acid (pinacol ester) were purchased from Sigma Aldrich company. Cesium carbonate and dimethyl sulfoxide were purchased from Aladdin company. All ordered chemicals were directly used without further purification.

A Bruker Vertex 70 FTIR spectrometer was used to test Fourier-Transformed Infrared (FT-IR) spectra. The samples were firstly dispersed and ground with KBr, and then prepared as disks. the FT-IR spectra range was 500–4000 cm^{-1}. Ultraviolet–visible spectra were collected by using UV–VIS-NIR spectrophotometer (UV-3600, Shimadzu Japan) at room condition. The testing wavenumber was previously set from 200 to 800 cm^{-1}. $BaSO_4$ was utilized as a sample base. In addition, the testing wavenumber was previously set from 200 to 800 cm^{-1}. ^1H NMR spectra of monomers were tested using a 400 MHz Bruker with an automated tune and matched multi-nuclei probe. ^{13}C cross-polarization magic angle spinning (CP/MAS NMR) spectra were acquired using solid-state techniques on a Bruker WB 400 MHz instrument. The experimental parameters included a contact time of 2 ms (ramp 100) and a pulse delay of 3 s. A Micromeritics ASAP 2020 M analyzer was used to evaluate the CO_2 and N_2 adsorption/desorption isotherms of Azo-CTPs at 273 and 298 K. The testing temperature was manipulated by recycling water bath with refrigeration equipment. Before the measurement, the Azo-CTPs were either vacuum-degassed (10^{-5} bar) or N_2 flowing heating at 110 °C overnight to remove the residential solvent. The thermal stabilities of Azo-CTP samples were evaluated by Thermogravimetric analysis (TGA) on Perkin-Elmer Pyrisl TGA. The TGA test was carried out under N_2 flowing atmosphere with a gradual heating rate of 10 °C min^{-1} from 25 to 800 °C. Powder X-ray diffraction (XRD) analysis was conducted by using Philips X' Pert Pro. High-resolution image of Azo-CTP samples of morphologies were evaluated by FEI Sirion 200 field emission-scanning electron microscope (FE-SEM).

2.2. Synthesis of Azo-CTPs

Typically, the polycondensation method of Azo-CTPs was to add 0.1175 g Terephthalamidine dihydrochloride (0.5 mmol), 0.3258 g cesium carbonate and 0.25 mmol M_0/M_1/mM_1/M_2 respectively in 10 mL dimethyl sulfoxide with two drops of deionized water to synthesize Azo-CTP_0/ Azo-CTP_1/ Azo-mCTP_1/ Azo-CTP_2. The reaction systems were then stirred and heated at 60 °C for 12 h, 80 °C for 12 h, 100 °C for 12 h, step by step, and then finally kept stabled at 150 ℃ for 3 days. After cooling down the reaction, the product precipitation was filtrated and washed with water, DMF and ethanol several times. The filtrated solid was also then further washed by stirring in 50 mL DMF, ethanol and water for 6 h respectively. Through the freezing-dry of the sample, the final product of Azo-CTP_0, Azo-CTP_1, Azo-mCTP_1 and Azo-CTP_2 powders were collected from related M_0, M_1, mM_1, M_2 reactions, respectively.

2.3. Visible light-driven CO_2 reduction measurement

The photocatalytic process was carried out under visible light irradiation from a 300 W Xe lamp ($\lambda > 420$ nm). 10 mg Azo-CTPs were firstly loaded with 3 wt% Pd and then reduced by $NaBH_4$. Such photocatalysts were then dispersed in 9 mL water and 1 mL TEOA solutions. The photocatalytic system was then bubbled by CO_2 gas flowing to remove oxygen and sealed at 25 °C by a recycling water system. The composition of the gas phase products in the photoreactor was analyzed via gas chromatography. The gas evolution rate of samples was determined by the hour of highest gas production.

3. Results and discussion

The monomer structures and synthetic routine are displayed in Scheme 1. In detail, aldehyde monomers with zero, one and two azobenzene groups were designed to adjust the azobenzene content in Azo-CTPs. Apart from that, compared to M_1, the aldehyde monomer shape of mM_1 was also changed to further tune the pore structure of Azo-mCTP_1. These aldehyde monomers were then reacted with amidine through a mild condensation reaction reported by Tan's group [17]. The successful fabrication of Azo-CTPs was demonstrated by Fourier Transform Infrared (FT-IR) analysis combined with solid carbon ^{13}C NMR spectra. The FT-IR results was shown in Fig. 1a. The broad peaks at 1350 and 1510 cm^{-1} were attributed to the stretching-vibration bands of C-N and C=N bonds in triazine rings, indicating the successful polycondensation reaction to form Azo-CTPs. Furthermore, another broad bands at 1410 cm^{-1} were assigned to the overlapping of introduced N=N bonding of azo groups and C=C bond of azo phenyl groups in azobenzene functionalized Azo-CTPs. Apart from that, the intensity of this peak was found to be enhanced with the increasing content of azobenzene pendants, which further reflected the successful modification of azobenzene group content in Azo-CTPs. Solid carbon ^{13}C NMR spectra of Azo-CTPs were further estimated to confirm the desired structure formations, As shown in Fig. 1b, the different peaks were respectively allocated to the corresponding carbon atoms, indicating the correct structure of designed Azo-CTPs. In detail, the small shoulder peaks located at 170 ppm suggested the presence of sp^2 carbon in triazine rings of Azo-CTPs, further supporting the successful polycondensation reactions. Apart from that, broad bands between 120 and 150 ppm were assigned to the aromatic carbons. Besides, powder X-ray diffraction patterns (Fig. 1c) revealed that all materials were generally amorphous.

The visible light-harvesting efficiency of Azo-CTPs was estimated by UV–vis diffuse reflectance measurement. As shown in Fig. 1d, all materials showed visible light absorption ability. Interestingly, with the increasing amount of integrated azobenzene pendants, visible light absorption onset expanded toward longer wavelengths, and absorption intensity was also enhanced to a higher level. Therefore, the installation of azobenzene groups could efficiently strengthen the visible light-

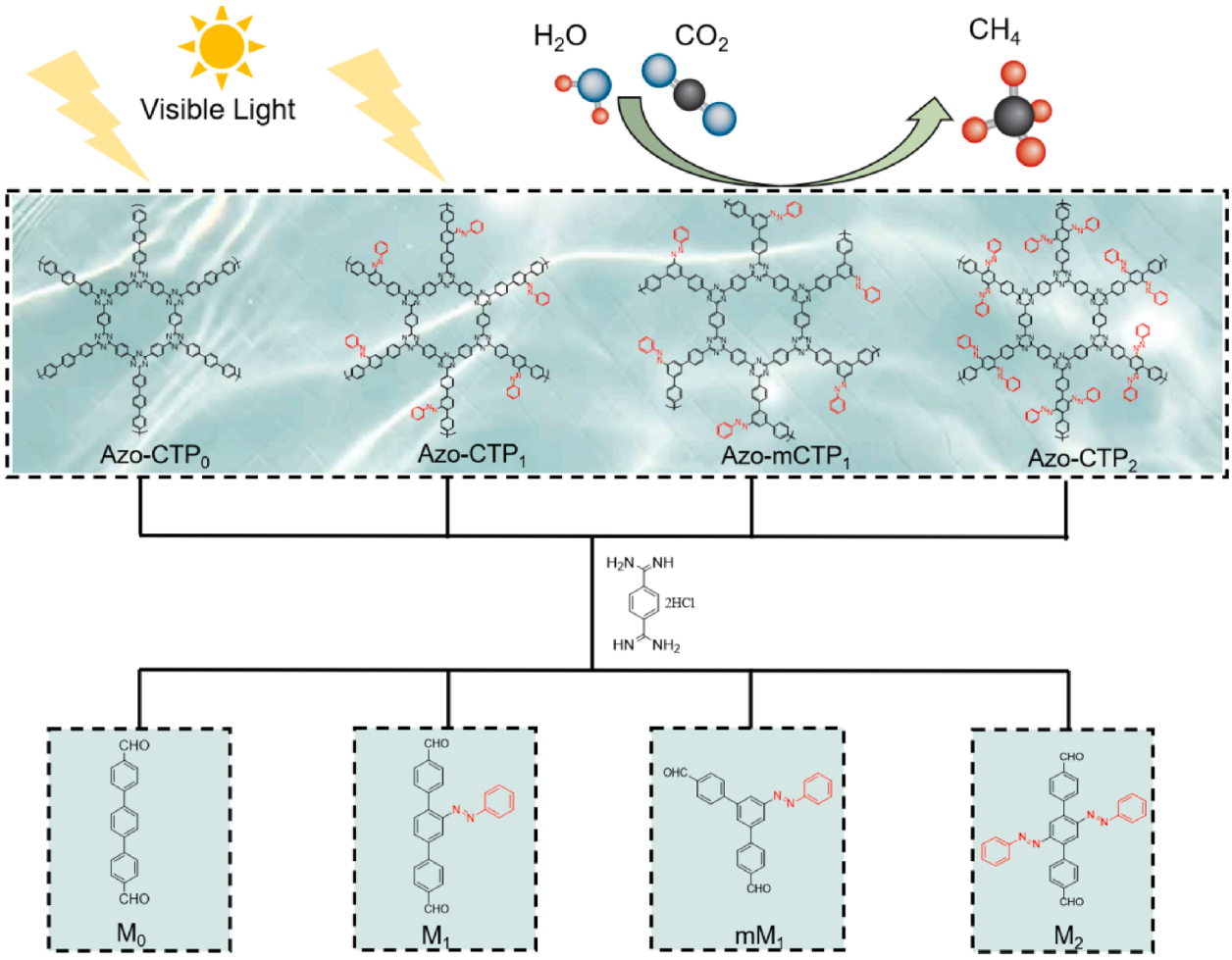

Scheme 1. Schematic illustration of synthetic procedure of Azo-CTPs and the application of the material for visible light-driven CO_2 reduction.

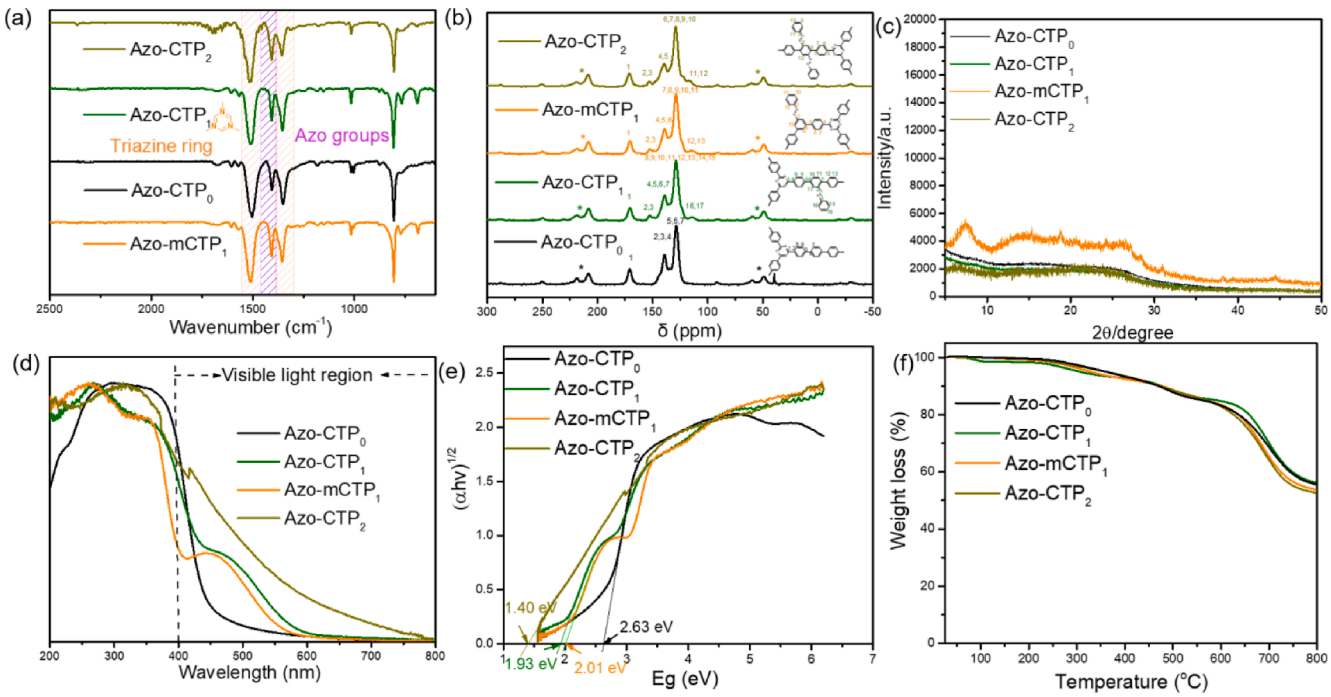

Fig. 1. (a) FT-IR (b) Solid-state ^{13}C NMR (c) powder X-ray diffraction patterns of Azo-CTPs. (d) UV–vis diffuse reflection spectra (DRS) of Azo-CTPs, (e) Band gap of Azo-CTPs. calculated from UV–vis DRS spectra. (f) Thermal gravimetric analysis curves of Azo-CTPs.

harvesting capability of Azo-CTPs, which is of vital importance to photocatalysis. Thermal gravimetric analysis (Fig. 1f) was then measured, and the results indicated that all Azo-CTPs could keep stable up to 300 °C. It is suggested that the introduction of azobenzene pendants did not affect the thermal stability of Azo-CTPs.

The porosities of all samples were evaluated by N_2 adsorption–desorption isotherms at 77 K (Fig. 2a). As a result, Azo-CTP_0 exhibited the highest surface area, up to 763 $m^2\ g^{-1}$. After azobenzene functionalization, the surface area of Azo-CTP_1 dropped to 525 $m^2\ g^{-1}$. This value further declined to 366 $m^2\ g^{-1}$ with the increasing azobenzene introduction amounts in Azo-CTP_2. The incorporated azobenzene pendants occupied specific volumes in pore channels of Azo-CTP_1 and Azo-CTP_2, which then led to a decrease in surface area. However, by changing the aldehyde monomer shape, Azo-mCTP_1 exhibited a much higher surface area than Azo-CTP_1, around 685 $m^2\ g^{-1}$. Pore size distribution was then analyzed by the density functional theory method (Fig. 2b). The micropore size of Azo-CTP_0, Azo-CTP_1 and Azo-CTP_2 was predominantly around 1.2 nm, with the value of Azo-mCTP_1 being smaller, around 0.8 nm. Apart from that, the mesopore and macropore can also be observed from related N_2 isotherm curves. Such multi kinds of pores are beneficial to the reactant transformation toward active sites during the photocatalytic reaction process.

Furthermore, CO_2 adsorption–desorption isotherms at 273 K and 298 K were measured to verify the CO_2 uptake performance of as-prepared samples. The results are shown in Fig. 2d and Fig. 2e. After the incorporation of azobenzene groups, Azo-CTP_1 demonstrated a slightly lower CO_2 adsorption amount than Azo-CTP_0, which might be attributed to the lower pore volume and surface area of Azo-CTP_1. However, after further increasing the introduction content of azo groups, the CO_2 uptake capacity of Azo-CTP_2 dramatically increased, around 41.6 $cm^3\ g^{-1}$ (1.86 mmol g^{-1}) at 273 K and 25.0 $cm^3\ g^{-1}$ (1.02 mmol g^{-1}) at 298 K. Considering the dipole-quadrupole interactivity between azo groups and CO_2 molecules, the lower surface area caused by the introduction of azo groups was made up by the CO_2 affinity of azo sites, which then led to the dramatically enhancing CO_2 uptake of Azo-CTP_2. These findings can be supported by the CO_2 adsorption heat calculated from the CO_2 sorption isotherms of three temperatures at 273 K, 285 K and 298 K. (Fig. 2c) It is suggested that the adsorption heat increased after azobenzene incorporation, further confirming the CO_2 affinity of azo groups. Furthermore, Azo-mCTP_1 showed the highest CO_2 uptake capacity, up to 48.2 $cm^3\ g^{-1}$ (2.15 mmol g^{-1}) at 273 K, due to the high BET surface area combined with CO_2 affinity azo groups. Such high CO_2 capture plays a key role in following photocatalytic CO_2 conversions for CO_2 access and transportation in pore channels.

Encouraged by the high surface area, enhanced visible light-harvesting capability and outstanding CO_2 uptake capacity of Azo-CTPs, these samples were applied in visible light-driven photocatalytic CO_2 reduction. Firstly, all Azo-CTPs materials were loaded with palladium as a cocatalyst and reduced with $NaBH_4$ before. The CO_2 adsorption performance of Azo-CTPs after Pd loading was also evaluated. As shown in Fig. 2f, the CO_2 uptake capacity of Pd loaded Azo-CTPs was only slightly decreased compared to the pure Azo-CTPs. The Pd loaded Azo-mCTP_1 still kept the highest uptake amount, around 6 times higher than the reported Pt-SA/CTF-1.[21] Apart from that, both scanning electron microscopy images (SEM) and field-emission transmission electron microscopy (FE-TEM) revealed that Azo-CTP_0 were primarily composed of stacking nanosheets, and the azobenzene functionalization did not affect such layered nanosheets morphology (Fig. 3(a-h)). In addition, TEM images also suggested the uniform dispersion of Pd nanoparticles on the Azo-CTP nanosheets with a particle size of around 2–5 nm. The energy-dispersive spectroscopy (EDS)-mapping images (Fig. 3(i-l)) indicated the element distribution of C, N, Pd, further demonstrating the uniform dispersion of Pd.

The X-ray photoelectronic spectra (XPS) spectra of Pd-loaded Azo-CTPs were then tested to determine the chemical states of the primary elements in as prepared Azo-CTP samples. As shown in Figure S2, the broad spectra of Azo-CTPs suggested the existence of C, N, Pd in the Azo-CTPs, indicating the successful loading of the cocatalyst. In addition, C 1 *s*, N 1 *s* and Pd 3*d* profiles of Pd loaded Azo-CTPs spectra were illustrated in Fig. 4. The C 1 s spectra of Azo-CTPs were deconvoluted into two peaks located at 285.2 and 287.3 eV, which could be assigned to graphite-like sp^2 carbon of C=C and N=C–N bond, respectively.

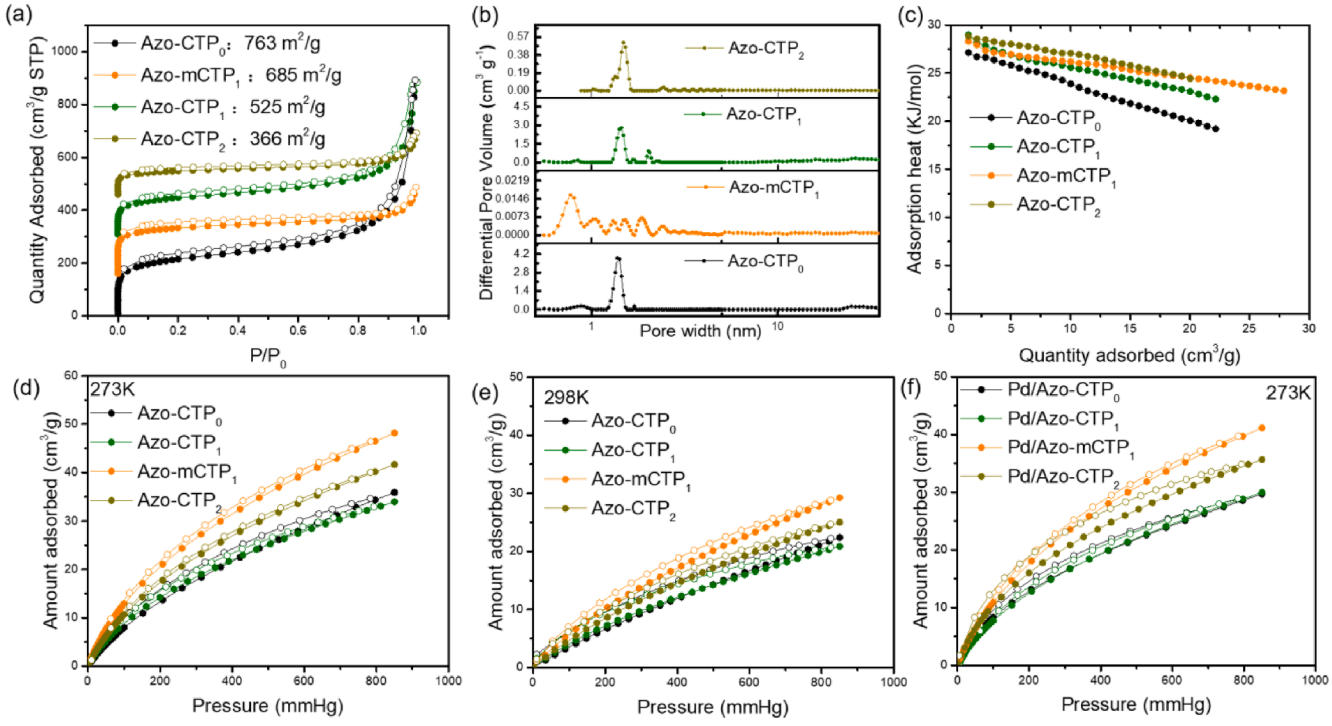

Fig. 2. (a) N_2 adsorption (closed circles) and desorption (open circles) isotherms (77 K) of Azo-CTPs. (b) Pore size distributions of Azo-CTPs. (c) Adsorption heat of Azo-CTPs. CO_2 adsorption isotherms at (d) 273 K and (e) 298 K of Azo-CTPs. (f) CO_2 adsorption isotherms at 273 K of Pd/Azo-CTPs.

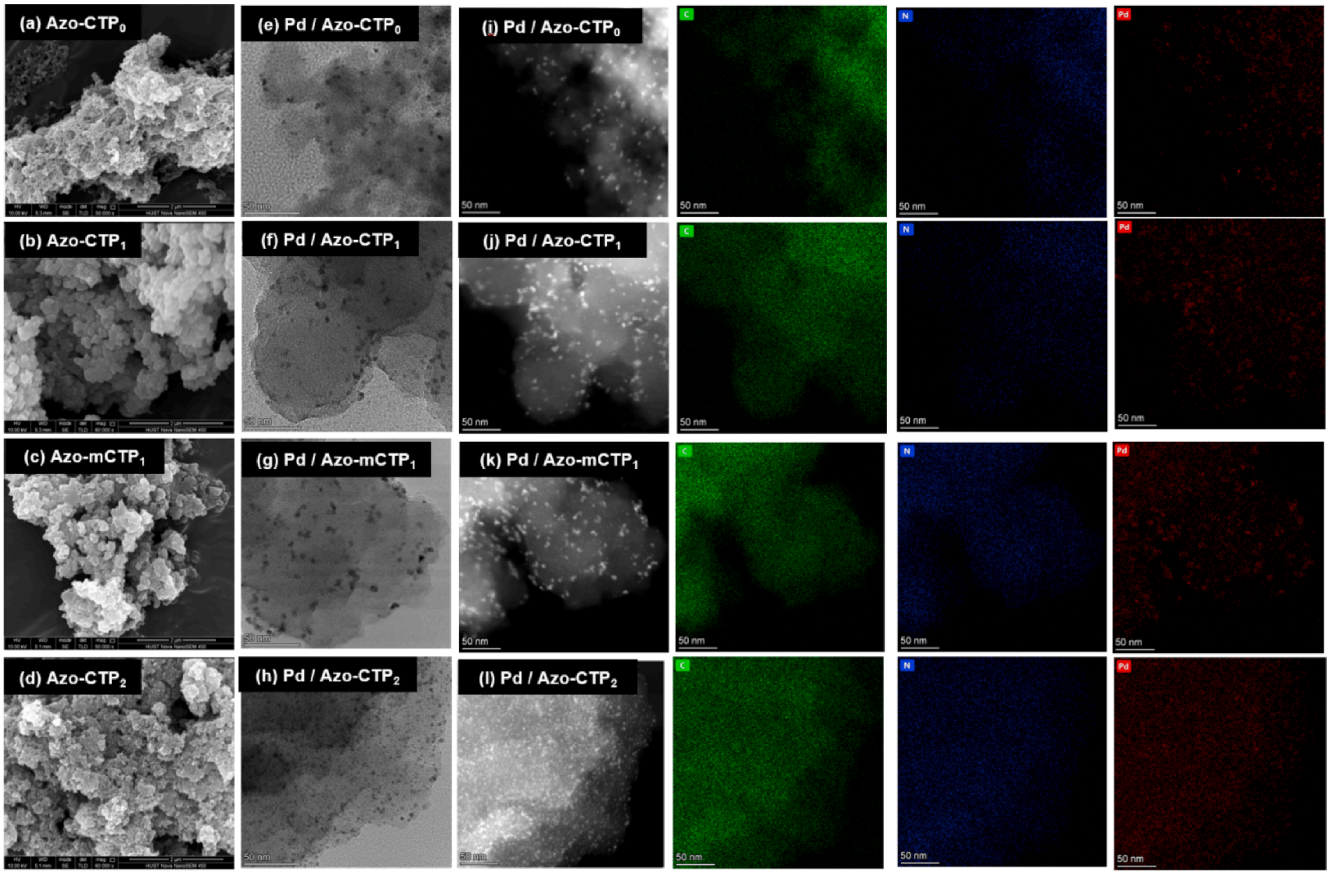

Fig. 3. (a-d) Scanning electron microscopy (SEM) of Azo-CTPs. (e-h) Field-emission transmission electron microscopy (FE-TEM) images of Pd loaded Azo-CTPs. (i-l) The high-angle annular dark-field (HAADF) and energy-dispersive spectroscopy (EDS)-mapping images of Pd loaded Azo-CTPs.

Compared to Azo-CTP$_0$, the increased intensity of N=C−N bond in Azo-CTP$_1$, Azo-mCTP$_1$ and Azo-CTP$_2$ could also be observed, further implying the successful incorporation of azo groups into CTP networks. The high resolution spectra of N 1 s in Azo-CTPs were resolved into two peaks 399.0 and 400.2 eV, respectively. The peak at 400.2 eV corresponded to pyrrolic nitrogen of C−NH−C or −N(N−(C))$_3$ resulting from the partial decomposition of Azo-CTPs, and the peak at 399.0 eV was attributed to the sp^2-hybridized nitrogen in pyridine C=N−C. More importantly, both compositions could be served as Lewis basic sites, which play a key role in the CO_2 adsorption process. In addition, the high-resolution Pd spectra in Azo-CTPs could be resolved into two main peaks with weak side shoulders. The peaks at 335.6 and 341.0 eV were originated from Pd(0) 3$d_{5/2}$ and Pd(0) 3$d_{3/2}$, indicating that the main valence state of Pd was Pd(0) because of the reduction process. The two weak shoulder peaks at 337.8 and 343 eV suggested the coexistence of the Pd^{2+} state in Azo-CTPs.

A photocatalytic CO_2 conversion experiment was carried out in a water solution system containing triethanolamine as a sacrificial agent. Such a water system avoids the dependence on using photosensitizers and common organic solvents such as acetonitrile and dimethylformamide, which greatly prevents the pollution of environmental hazards. The photocatalytic results are depicted in Fig. 5a. Under visible light irradiation, CO and CH_4 were detected as primary reduction products of Azo-CTP$_1$ and Azo-mCTP$_1$ under the same photocatalytic conditions. Compared to Azo-CTP$_0$ and Azo-CTP$_2$, Azo-CTP$_1$ and Azo-mCTP$_1$ suggested a remarkably higher CH_4 evolution rate. Apart from that, the selectivity to CH_4 in Azo-CTP$_1$ and Azo-mCTP$_1$ could reach up to 97 %. Since the eight-electron reduction process is the toughest way in kinetics than the two-electron process for CO production and other lower electron reduction approaches, such high selectivity of CH_4 confirmed the superior CO_2 reduction activity of Azo-mCTP$_1$ and Azo-CTP$_1$. In detail, Azo-CTP$_1$ indicated an 8.0 μmol $g^{-1}h^{-1}$ evolution rate of CH_4, which is nearly four times higher than Azo-CTP$_0$. These results suggest that the azobenzene installation can dramatically increase the CO_2 reduction rate of Azo-CTP$_0$. However, further increasing the installation amounts in Azo-CTP$_2$ leads to decreased CO_2 photocatalytic activity. Apart from that, by changing the monomer shape of Azo-CTP$_1$, Azo-mCTP$_1$ even showed a higher CH_4 evolution rate, up to 8.2 μmol $g^{-1}h^{-1}$. The certain ordered structure of Azo-mCTP$_1$ may contribute to its highest photocatalytic activity. As shown in Table S1, a comprehensive summary of the photocatalytic CO_2 reduction performance of reported COF materials under visible light irradiation is listed. Although the photocatalytic performance of COF materials in the organic solvent is much higher than that of the water system, they still face easy self-degradation and environmental hazard issues. However, Pd/Azo-mCTP$_1$, exhibits comparable photocatalytic activities and high CH_4 evolution selectivity in the reported water system, which indicates the attractive potential for applications in environmentally friendly conditions [21].

Apart from that, such high activity process can be further recycled for four runs with slight deactivation (Fig. 5b), indicating the excellent recyclability of the Azo-mCTP$_1$ catalytic system. We have also performed FT-IR analysis on the recycled sample. The results, presented in Figure S8, indicated that the locations of peaks in the FT-IR spectra remain unchanged after 16 h of photocatalytic reaction. This further supports the superior stability of Pd/Azo-mCTP$_1$. To investigate the potential agglomeration of Pd particles during the cycle reaction, field-emission transmission electron microscopy (FE-TEM) images of Pd-loaded Azo-CTP$_1$ were estimated both before and after the catalytic cycle reaction. The results are shown in Figure S9. The particle sizes of Pd in the corresponding TEM images were manually measured by using Image J. The results of these measurements have been incorporated into Figure S10, where it is evident that the particle size of Pd experienced a

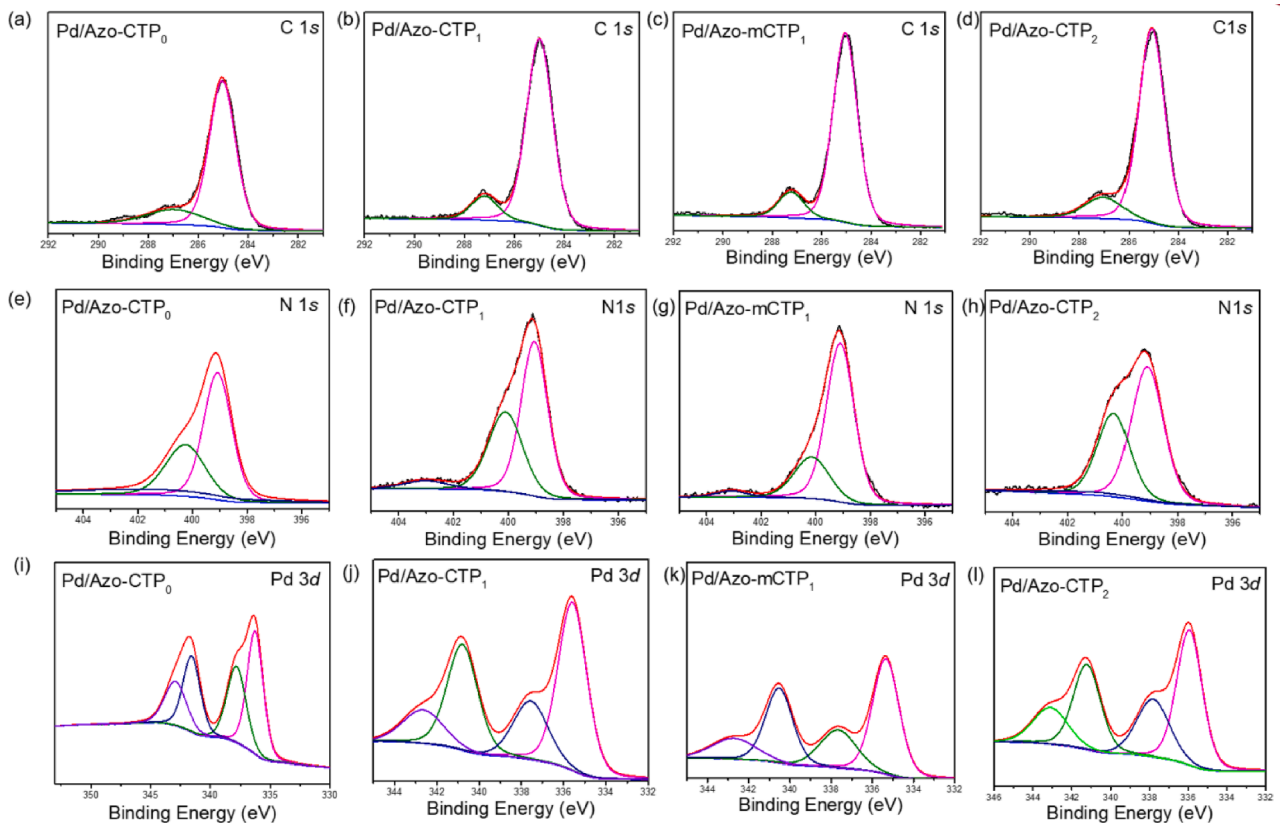

Fig. 4. C 1 s, N 1 s and Pd 3d profiles of Pd loaded (a, e, i) Azo-CTP_0, (b, f, j) Azo-CTP_1, (c, g, k) Azo-$mCTP_1$ and (d, h, l) Azo-CTP_2.

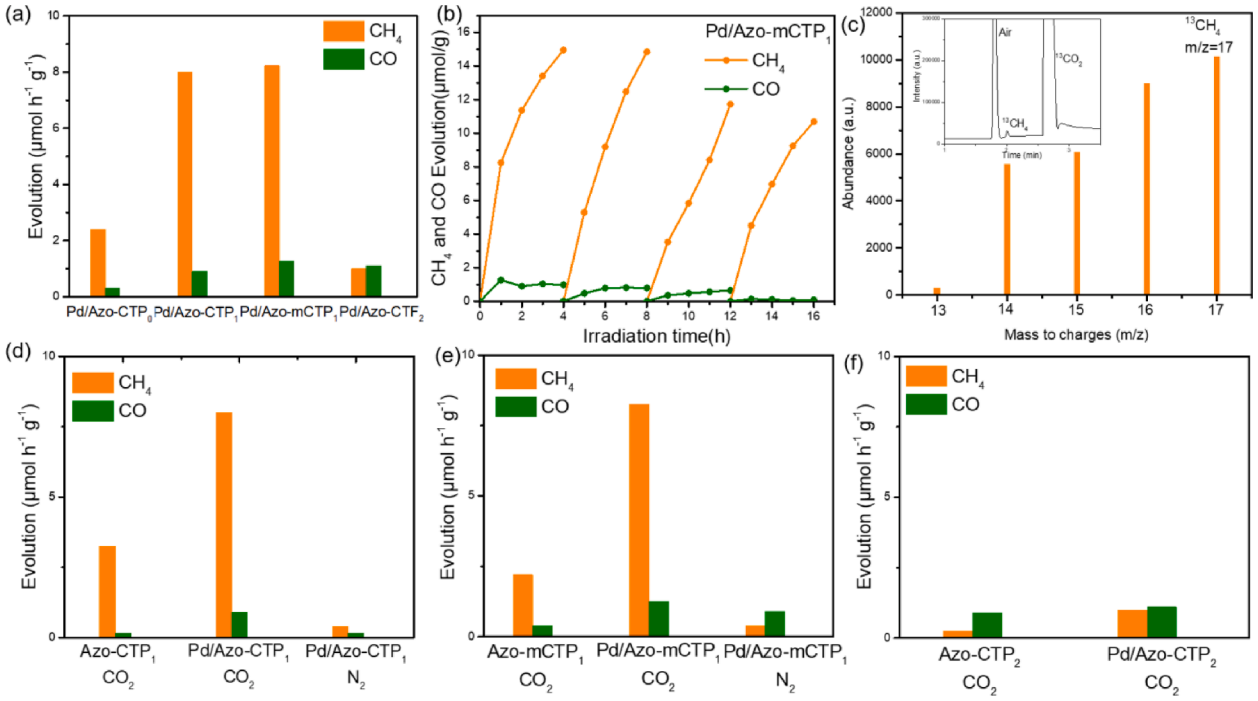

Fig. 5. (a) Photocatalytic CO_2 reduction rates of Pd/Azo-CTPs under visible light irradiation. (b) Recyclability of Pd/Azo-$mCTP_1$ for the photocatalytic CO_2 conversion. (c) GC–MS spectra of gas products after the photocatalytic reaction over Pd/Azo-$mCTP_1$. The isotopically labeled $^{13}CO_2$ was used as a substrate under normal experimental conditions. The CO_2 reduction activities under pure nitrogen atmosphere of Pd loaded (d) Azo-CTP_1 and (e) Azo-$mCTP_1$. CO_2 reduction activities of pure and Pd loaded (f) Azo-CTP_2.

slight increase after the cycle. This observation supports the notion that Pd particles agglomerated during the photocatalytic cycle reaction. This also align with the fact that the photocatalytic efficiency slightly decreased as the longer time irradiation during the cycles.

Additionally, a control experiment was performed to ensure the carbon origin of produced CH_4. The photocatalytic process of Azo-mCTP$_1$ and Azo-CTP$_1$ were conducted under the high purity nitrogen atmosphere with other conditions kept the same, and the results are shown in Fig. 5(d) and (e). As a result, negligible CH_4 was detected after the same time visible light irradiation. Apart from that, the isotopic reactions were further conducted to track the origin of the products by using GC–MS. The results are presented in Fig. 5 (c). The chromatogram clearly shows separate peaks for CH_4 (1.9 min) and CO_2 (2.3 min) in the Total Ion Chromatogram (TIC). To confirm the source of CH_4, we analyzed the corresponding MS spectra. The obtained spectra for CH_4 align with the fragment ions generated from $^{13}CH_4$, namely $^{13}CH_4^+$ ($m/z = 17$), $^{13}CH_3^+$ ($m/z = 16$), $^{13}CH_2+$ ($m/z = 15$), $^{13}CH^+$ ($m/z = 14$), and $^{13}C^+$ ($m/z = 13$). This conclusive evidence demonstrated that the carbon source of generated CH_4 was originally from CO_2 instead of the decomposition of the photocatalytic system. In addition, the photocatalytic CO_2 reduction performance when using the pure Azo-CTPs was estimated. Among them, even pure Azo-CTP$_1$ and Azo-mCTP$_1$ still enable the reduction of CO_2 to CH_4 via eight electron ways with high selectivity (Fig. 5(d) and (e)). In addition, the evolution rates were much higher than Azo-CTP$_2$ (Fig. 5(f)) and Azo-CTP$_0$ (Figure S3). These results further confirm the influence of azobenzene functionalization and integration amounts on Azo-CTP$_0$.

To further elucidate the photocatalytic CO_2 reduction activities, the optical properties of Azo-CTPs were studied and compared. Photocurrent responses of these samples were estimated when periodically on/off irradiated by visible light (Fig. 6a). Compared with Azo-CTP$_0$ and Azo-CTP$_2$, significantly higher photocurrent intensity of Azo-mCTP$_1$ and Azo-CTP$_1$ was observed, with Azo-mCTP$_1$ even slightly stronger. It is demonstrated that the photoinduced charge separation and transformation in Azo-CTP$_1$ and Azo-mCTP$_1$ have been accelerated, supporting the remarkably higher photocatalytic performance of Azo-CTP$_1$ and Azo-mCTP$_1$. In addition, electrochemical impedance spectroscopy (EIS) analysis was also investigated under visible light irradiation to study the photogenerated charge mobility in Azo-CTP samples. As shown in Fig. 6b, Azo-mCTP$_1$ possessed the lowest resistance among Azo-CTPs, followed by Azo-CTP$_1$, implying the faster electron transfer of Azo-mCTP$_1$ and Azo-CTP$_1$. The photoluminescence spectra of Azo-CTPs was also estimated to elucidate the light-induced charge recombination rate (Fig. 6 (c)). The results revealed that Azo-CTP$_0$ exhibits a high emission intensity. Importantly, this intensity experiences a significant decrease after the azobenzene functionalization. This observation strongly suggests that the azobenzene functionalization effectively prevents charge recombination, which also aligns with the high photocatalytic activity of Azo-CTP$_1$ and Azo-mCTP$_1$. Therefore, the higher charge separation and transformation rate of Azo-mCTP$_1$ successfully contribute to the highest superior photocatalytic CO_2 reduction activity.

Band gap structures with related conduction band and valence band positions were also obtained via Mott-Schottky combined with UV–vis DRS analysis. Band gap values of Azo-CTPs were first calculated from UV–vis DRS. As depicted in Fig. 1e, the more integrated amount of azobenzene pendants led to narrower band gap values, reflecting a broader visible light response range in UV–vis DRS spectra. Furthermore, the flat band potentials of Azo-CTPs were measured via Mott-Schottky analysis (Fig. 7 (b-e)). The positive slope of Mott-Schottky plots indicated that all as-prepared materials were typical n-type semiconductors. Since conduction band positions were extremely close to flat band potentials for n-type semiconductors, the conduction band of Azo-CTPs was determined and shown in Fig. 7a. Notably, all conduction band edges of Azo-CTPs are more negative than E(CO_2/CO vs NHE) and E(CO_2/CH_4 vs NHE), implying that photoinduced electrons of visible light irradiated Azo-CTPs can theoretically reduce the adsorbed CO_2 to CO and CH_4. These further supported the capability of all Azo-CTPs for photocatalytic CO_2 conversion to CH_4 and CO. Moreover, Azo-mCTP$_1$ showed the highest conduction band positions among Azo-CTPs, around −1.02 V, which was followed by Azo-CTP$_1$, around −0.98 V. Since higher conduction band positions are related to a stronger driving force toward CO_2 reduction, Azo-mCTP$_1$ theoretically embraces the enhanced photocatalytic CO_2 reduction ability. This supports the photocatalytic results that Azo-mCTP$_1$ suggested the highest CH_4 evolution rate. Therefore, different azobenzene functionalization toward Azo-CTP$_0$ successfully tuned the band gap structure and then optimized the photocatalytic CO_2 performance.

Based on the abovementioned discussion, the possible mechanism of photocatalytic CO_2 reduction process over Pd/Azo-CTPs catalyst was proposed. Upon visible light irradiation, Pd/Azo-CTPs were excited to generate the CB electrons (e^-) and VB hole (h^+) pairs. Subsequently, the photogenerated hole (h^+) was then quenched by the sacrificial reagent of TEOA, and the CB electrons (e^-) were migrated to Pt active species. Such electron's immigration from Azo-CTPs to Pd nanoparticles also prevents the recombination of charge carriers and accelerates the charge transformation. The loaded Pd can be regarded as a cocatalyst in this catalyst system. Introducing Pd species into Azo-CTPs could harvest more visible-light photons and produce more photogenerated carriers than pristine Azo-CTPs. The photo generated electrons will be promptly transferred to Pd active species. This is also the reason that both the Pd loaded Azo-mPCTP$_1$ and Azo-CTP$_1$ suggested dramatically higher photocatalytic activity than pure mPCTP$_1$ and Azo-CTP$_1$. With more Pt active species formation, CO_2 molecules were adsorbed into CTPs and interacted with the photo reduced Pd species to form CO_2^-. Finally, the activated $\cdot CO_2^-$ was reacted with protons from H_2O and transformed into CH_4 through a multistep reduction process, such as breaking the C-O bonds and the formation of C–H bonds. Moreover, the high CO_2 adsorbed capacity of Pd/Azo-CTPs was also of vital importance to promote the formation of Pd-CO_2 adduct and then enhance the methane evolution performance.

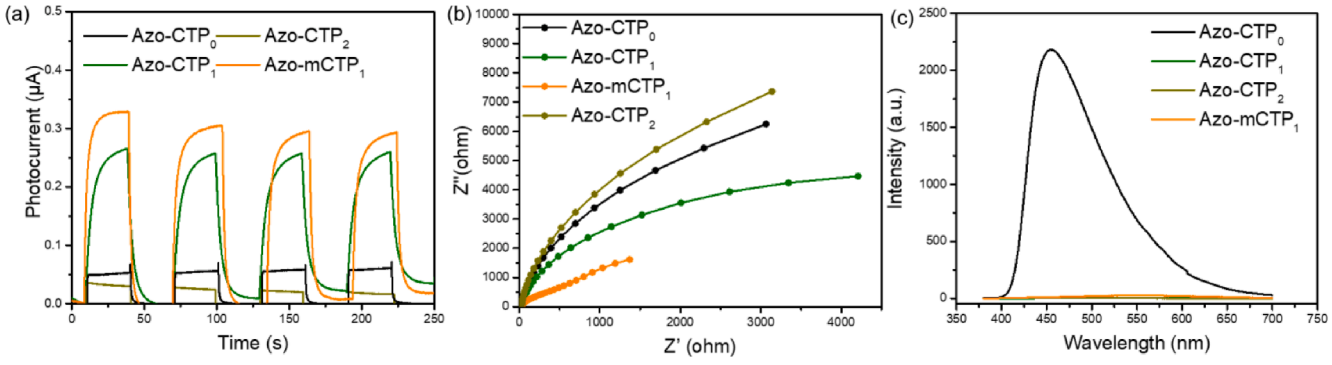

Fig. 6. (a) Photocurrent response, (b) electrochemical impedance spectroscopy (EIS) Nyquist plots and (c) Steady-state photoluminescence spectra of Azo-CTPs.

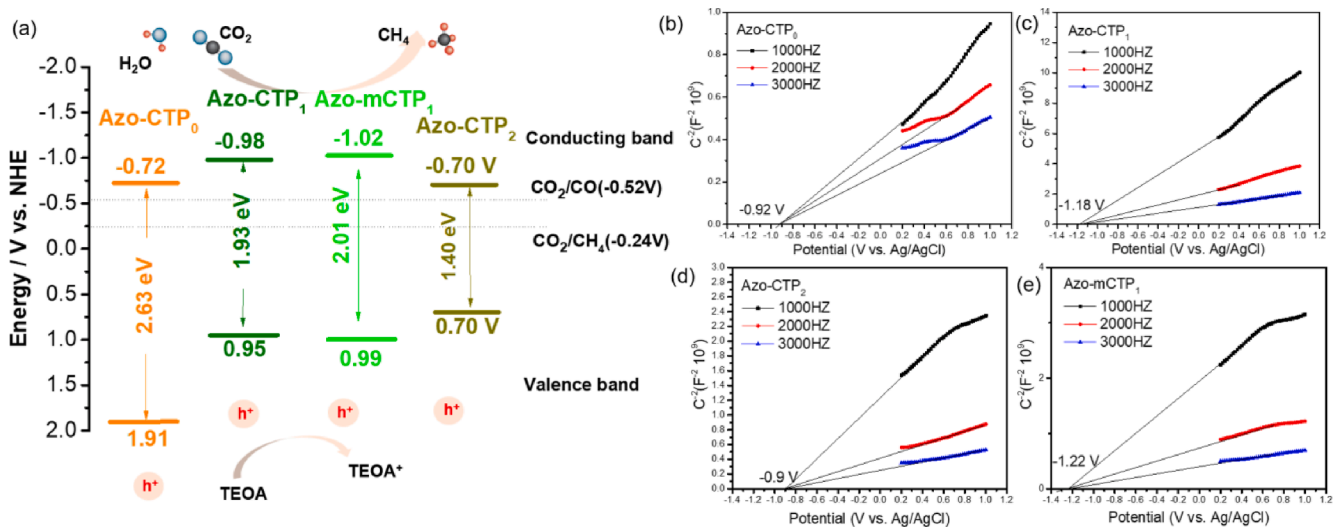

Fig. 7. (a) Band gap structures of Azo-CTPs. (c-e) Mott-Schottky analysis of Azo-CTPs.

4. Conclusion

A series of azobenzene functionalized Azo-CTPs were successfully fabricated via the polycondensation reactions between amidines and different amounts of azobenzene contained aldehyde monomer. Both the CO_2 uptake capacity and the band gap structure were also successfully tuned by the different amounts of azobenzene group installation and different shapes of aldehyde monomer. Among them, Azo-mCTP$_1$ suggested the highest CO_2 uptake capacity up to 48.2 $cm^3\ g^{-1}$ (2.15 mmol g^{-1}), and a 4 times higher CH_4 evolution rate than Azo-CTP$_0$ under visible light irradiation with high selectivity up to 97 %. Such azobenzene functionalized approach of CTPs not only provides a promising strategy for precise modification of organic photocatalysts but also delivers a new insight for enhancing photocatalytic conversion efficiency. Furthermore, other photocatalytic reactions also can be expected through this azo-based functionalization method.

CRediT authorship contribution statement

Qi Huang: Writing – review & editing, Writing – original draft, Visualization, Validation, Software, Methodology, Investigation, Formal analysis, Data curation, Conceptualization. **Zhen Zhan:** Writing - Review & Editing, Formal analysis. **Yuanting Qiao:** Writing – review & editing, Formal analysis. **Xueting Pan:** Writing – review & editing. **Shaojun Xu:** Writing – review & editing. **Bien Tan:** Conceptualization, Writing – review & editing, Resources, Supervision. **Chunfei Wu:** Conceptualization, Writing – review & editing, Resources, Supervision, Funding acquisition.

Declaration of competing interest

The authors declare that they have no known competing financial interests or personal relationships that could have appeared to influence the work reported in this paper.

Data availability

The data that has been used is confidential.

Acknowledgement

The authors sincerely appreciate the financial support from the China Scholarship Council. We also appreciate the isotopic GC-MS support from Center for Experimental Chemistry, School of Chemistry and Chemical Engineering, Huazhong University of Science and Technology. This project has received funding from the European Union's Horizon 2020 research and innovation programme under the Marie Skłodowska-Curie grant agreement No 823745.

Appendix A. Supplementary material

Supplementary data to this article can be found online at https://doi.org/10.1016/j.fuel.2023.130646.

References

[1] Inoue T, Fujishima A, Konishi S, Honda K. Nature 1979;277:637–8.
[2] Chen J, Xu Y, Liao P, Wang H, Zhou H. Carbon Capture Sci Technol 2022;4:100052.
[3] Soltani SM, Lahiri A, Bahzad H, Clough P, Gorbounov M, Yan Y. Carbon Capture Sci Technol 2021;1:100003.
[4] Guo K, Zhu X, Peng L, Fu Y, Ma R, Lu X, et al. Chem Eng J 2021;405:127011.
[5] Yao X, Chen K, Qiu L, Yang Z, He L. Chem Mater 2021;33:8863–72.
[6] Wang S, Guan B, Lou X. Energy Environ Sci 2018;11:306–10.
[7] Rastgaran A, Fatoorehchi H, Khallaghi N, Larimi A, Borhani TN. Carbon Capture Sci Technol 2023;8:100118.
[8] Mei Y, Yuan N, Liu Y, Zhang X, Lin B, Zhou Y. Carbon Capture Sci Technol 2021;1:100016.
[9] Liu M, Liping Guo S, Jin BT. J Mater Chem A 2019;7:5153–72.
[10] Zhu S, Qi Q, Fang Y, Zhao W, Wu M, Han L. Cryst Growth Des 2017;18:883–91.
[11] Niu F, Tao L, Deng Y, Gao H, Liu J, Song W. New J Chem 2014;38:5695–9.
[12] Kuecken S, Acharjya A, Zhi L, Schwarze M, Schomacker R, Thomas A. Chem Commun 2017;53:5854–7.
[13] Wang G, Leus K, Jena HS, Krishnaraj C, Zhao S, Depauw H, et al. J Mater Chem A 2018;6:6370–5.
[14] Gu C, Liu D, Huang W, Liu J, Yang R. Polym Chem 2015;6:7410–7.
[15] Hug S, Stegbauer L, Oh H, Hirscher M, Lotsch BV. Chem Mater 2015;27:8001–10.
[16] Niu Q, Cheng Z, Chen Q, Huang G, Lin J, Bi J, et al. ACS Sustainable Chem Eng 2021;9:1333–40.
[17] Guo L, Niu Y, Xu H, Li Q, Razzaque S, Huang Q, et al. J Mater Chem A 2018;6:19775–81.
[18] Yan Y, Fang Q, Pan J, Yang J, Zhang L, Zhang W, et al. Chem Eng J 2021;408:127358.
[19] Zhong H, Hong Z, Yang C, Li L, Xu Y, Wang X, et al. ChemSusChem 2019;12:4493–9.
[20] Bi J, Xu B, Sun L, Huang H, Fang S, Li L, et al. ChemPlusChem 2019;84:1149–54.
[21] Huang G, Niu Q, Zhang J, Huang H, Chen Q, Bi J, Wu L. Chem Eng J 2021;427:131018.
[22] Huang W, Huber N, Jiang S, Landfester K, Zhang KAI. Angew Chem Int Ed 2020;59:18368–73.
[23] Lu C, Yang J, Wei S, Bi S, Xia Y, Chen M, et al. Adv Funct Mater 2019;29:1806884.
[24] Patel HA, Je SH, Park J, Chen DP, Jung Y, Yavuz CT, et al. Nat Commun 2013;4:1357.
[25] Patel HA, Je SH, Park J, Jung Y, Coskun A, Yavuz CT. Chemistry 2014;20:772–80.
[26] Lu J, Zhang J. J Mater Chem A 2014;2:13831–4.
[27] Arab P, Rabbani MG, Sekizkardes AK, İslamoğlu T, El-Kaderi HM. Chem Mater 2014;26:1385–92.

[28] Wang Q, Wang J, Wang JC, Hu X, Bai Y, Zhong X, et al. ChemSusChem 2021;14:1131–9.
[29] Xu T, Li Y, Zhao Z, Xing G, Chen L. Macromolecules 2019;52:9786–91.
[30] Xu Z, Cui Y, Young DJ, Wang J, Li H, Bian G, et al. J CO_2 Util 2021;49:101561.
[31] Wang J, Zhang Y. Green Chem 2016;18:5248–53.